Multi-Objective Cascaded Controller Design for Multi-Output DC-DC Converter in Grid-Connected PV System

Ouijdane Arich[1,*], *Abdelmajid* Abouloifa[1], *Amine* El Boudali[1], and *Nouhaila* Hourri[1]

[1]Energy and Electrical Systems Laboratory, ENSEM, Hassan II University, Casablanca, Morocco

Abstract. As renewable energy becomes increasingly essential to global energy strategies, grid-connected photovoltaic (PV) systems are gaining prominence. However, these systems introduce challenges related to power quality and system stability. This paper presents a unified nonlinear cascaded control strategy tailored for a multilevel single-input dual-output (SIDO) boost converter-based grid-connected PV system. The proposed approach is aimed at integrating the sliding mode control (SMC) for both maximum power point tracking (MPPT) and power factor correction (PFC) tasks, while a filtered proportional-integral (PI) controller is employed to stabilize DC voltage regulation. This combination control framework ensures these objectives under varying environmental conditions, all while taking advantage of multilevel conversion, such as reduced component stress and high voltage gain without transformers. Simulations studied within the MATLAB/Simulink environment confirm the proposed approach effectiveness, demonstrating reliable performance and enhanced improvements in system stability compared with the widely conventional approach.

1 Introduction

Global energy demand has been rapidly increasing, coupled with the depletion of fossil fuel reserves, intensifying the need for clean and sustainable energy solutions. Renewable energy sources have become central to modern energy strategies, with solar photovoltaic (PV) energy emerging as one of the most promising options due to its abundance, sustainability, and low environmental impact [1]. This work focuses on PV systems, which convert solar radiation directly into electrical power and are now widely used in the residential, commercial, and industrial sectors to power lighting, home appliances, and electric vehicles. These systems can operate either in standalone configurations or integrated into the electrical grid [2, 3]. The latter are particularly gaining popularity.

The power conversion stage is typically based on a high-gain DC-DC converter, needed to step up the low output voltage of the PV modules. However, conventional topologies such as classical boost, interleaved, or cascaded converters suffer from high ripple, large duty cycles, and component stress, limiting their efficiency and compactness [4, 5]. To address these limitations, multilevel DC-DC converter topologies have emerged as a promising solution [6]. In particular, the multilevel single-input multiple-output (SIMO) boost converter used in this work offers high voltage gain, low voltage stress, and continuous input current, without the need for a transformer. It combines a conventional boost structure with switched capacitor

*e-mail: ouijdane.arich-etu@etu.univh2c.ma

networks [7]. Its ability to improve efficiency and modularity makes the proposed multilevel boost converter (MLBC) especially well suited for renewable energy conversion [8, 9].

The framework of studies on SIMO-MLBCs for standalone and grid-connected PV systems has mainly relied on conventional control strategies. Pulse width modulation (PWM) is commonly used to reduce output voltage and current harmonics, which improves power quality [10]. However, PWM lacks the ability to adapt to changes. To achieve feedback control, many works have often integrated it with proportional-integral (PI) controllers because they are simple [11]. Nevertheless, PI controllers struggle with the nonlinear nature of SIMO-MLBCs. They are also sensitive to disturbances and parameter variations. Advanced approaches, such as fractional order PID (FOPID), offer better robustness and greater tuning flexibility [12]. However, their implementation is computationally intensive and complex. To address these challenges, more advanced methods such as model predictive control (MPC) and backstepping control have been introduced [9, 13]. MPC offers optimization and constraint handling capabilities [14], but still suffers from a high computational burden and real-time implementation challenges, especially in fast-switching power electronics. Backstepping control [8, 9], on the other hand, ensures Lyapunov-based stability and smooth tracking for strict-feedback nonlinear systems [8], yet becomes mathematically intensive and less practical when extended to multiple-output converters with complex interdependencies.

These limitations motivate the need for robust and low-complexity control strategies, such as sliding mode control (SMC), which offers strong robustness to model uncertainties, finite-time convergence, and efficient handling of nonlinear multi-output systems. Building on this need, this present work introduces a novel application of the SMC strategy specifically tailored for SIMO MLBC-based PV systems, a combination that, to the best of our knowledge, has not yet been reported in the literature. Therefore, the proposed controller not only guarantees accurate multi-output voltage regulation and effective MPPT but also introduces a new and resilient control framework for advancing the state of the art in nonlinear power converter technologies for renewable energy applications.

This paper is aimed at presenting the control of a single-phase grid-connected PV system integrating an adaptive stage based on an MLBC, which is designed to accomplish three control goals: i) Extract maximum energy by regulating the PV panel voltage, ii) Achieve perfect power factor correction (PFC) by controlling the grid current, and iii) Ensure stability and quality of energy injection by regulating the DC-link voltage. To achieve these goals, a cascaded nonlinear control strategy is proposed. It integrates the P&O algorithm to define the MPPT voltage reference and employs SMC for both the PV voltage and grid current loops [15]. Additionally, a filtered PI controller is implemented in the outer loop to regulate the DC-link voltage, ensuring smooth dynamic response and robustness under varying operating conditions.

The rest of this paper is organized as follows: Section 2 presents the description and the mathematical average modeling. Section 3 explains the controller design of the overall system. Section 4 provides the simulation results using MATLAB/Simulink, and Section 5 wraps up the paper.

2 Description of the Power Stage and Modeling

The proposed MLBC-SIDO PV system and its control-oriented model are detailed in this section.

2.1 Power Stage Description

The electrical diagram of the proposed plant is illustrated in the figure. 1 is a grid-connected photovoltaic (PV) power conversion setup designed to allow energy conversion from the solar panel to be efficient. The special multilevel boost converter (MLBC) with an inductor L and switch S_1 (controlled by μ_1) is vital for boosting the DC voltage generated by the PV panel, simultaneously charging multiple DC-link capacitors ($C_{1,2}$) through a diode network ($D_{1,2,2'}$), optimizing input for the subsequent H-bridge inverter, which consists of two IGBTs S_2 and $\bar{S}_2$ (controlled by μ_2) for generating a modulated AC voltage, and is connected through a filter inductor L_g, r_g before injecting it into the grid.

This structure supports MPPT control, DC-link regulation, and high-quality power injection, making it suitable for renewable energy integration. The mathematical modeling of the subsystems is discussed in Sect 2.2.

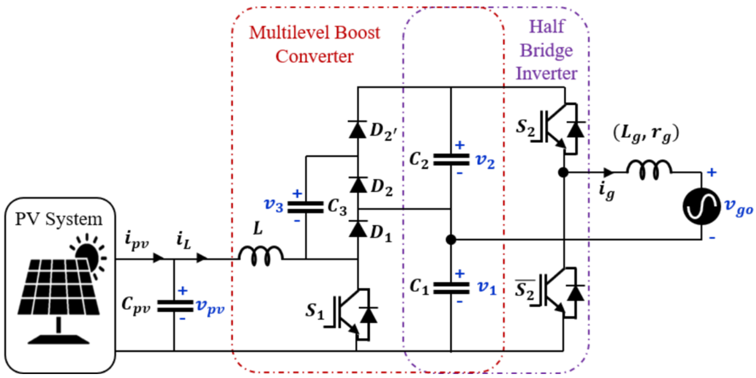

Figure 1. Detailed circuit of the proposed MLBC-based grid-tied PV system.

2.2 Model Derivation of the Power Stage

An equivalent circuit representation that depends on the switching behavior of both the SIDO boost converter and the single-phase HBI [9] is used to create the nonlinear static average model. The control input for an MLBC stage is controlled by a PWM signal, denoted as μ_1, using the set's values $\{0, 1\}$. Likewise, the inverter is also driven under a PWM-based control input μ_2, taking the finite set $\{-1, 1\}$, representing the switching sequence of the inverter legs.

Applying the widely recognized Kirchhoff's rules, the entire system model of the dynamic average can be written as follows:

$$C_{pv}\frac{dx_1}{dt} = \bar{i}_{pv} - x_2 \tag{1. a}$$

$$L\frac{dx_2}{dt} = x_1 - (1-u_1)\frac{x_3}{2} \tag{1. b}$$

$$C\frac{dx_3}{dt} = (1 - 2u_1 - 3u_2)\,\frac{x_5}{4} + (1-u_1)\,x_2 \tag{1. c}$$

$$C\frac{dx_4}{dt} = -(3 - u_2 + 2u_1u_2)\,\frac{x_5}{4} - (1-u_1)\,x_2 \tag{1. d}$$

$$L_g\frac{dx_5}{dt} = -r_gx_5 - \bar{v}_{go} + \frac{x_4}{2} + \frac{x_3}{2}u_2 \tag{1. e}$$

EPJ Web of Conferences **380**, 02009 (2026) https://doi.org/10.1051/epjconf/202638002009
ICISCT'25

where x_1, x_2, x_3, x_4, and x_5 represent the mean values of v_{pv}, i_L, v_s, v_d, and i_g. The control inputs μ_1 and μ_2 denote the duty cycles of the switches. The signals v_s and v_d correspond to the sum and difference of the capacitor voltages, respectively.

3 Sliding Mode Control Strategy Design

In this section, a nonlinear cascaded control strategy based on sliding mode control (SMC) is developed to ensure the threefold objectives previously outlined. The design steps and a comprehensive description of each loop are given in the subsequent subsections. The overall control structure, including proposed regulation loops, is illustrated in figure 2.

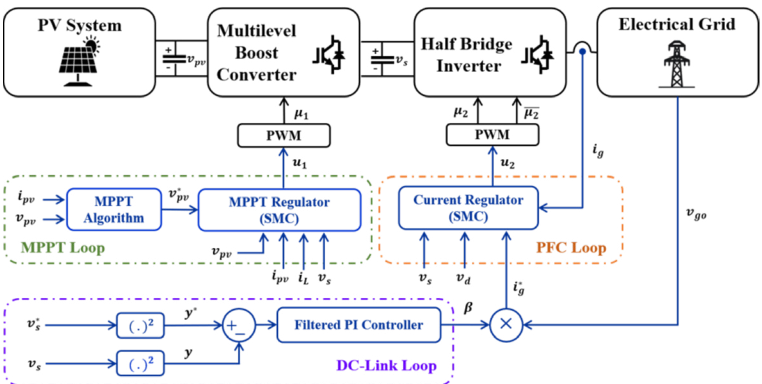

Figure 2. Block diagram of the proposed cascaded control strategy.

3.1 Design of MPPT Regulator

Searching for the optimal point becomes essential, as climate conditions cause fluctuations that affect the voltage and current delivered by the PV array. To address this, the proposed system employs an MPPT strategy that combines the simplicity of the perturb and observe (P&O) algorithm with the robustness of SMC. Once the voltage reference is determined, the proposed technique is designed to regulate the PV voltage x_1 to follow its reference value x_1^*. The control law is derived using a Lyapunov-based approach to guarantee both system robustness and finite-time convergence.

The MLBC control input is defined as:

$$u_1 = u_1^{Eq} + u_1^N \tag{2}$$

where u_1^{Eq} denotes the equivalent control, which keeps the system trajectory on the sliding surface, while the discontinuous control u_1^N is responsible for driving the system state towards the sliding manifold. This combined strategy allows for accurate MPPT while maintaining system stability and high dynamic performance.

To control how the error evolves, one defines the following sliding surface:

$$S = \left(\frac{d}{dt} + \delta\right)^{n-1} e \tag{3}$$

here, δ is a positive design parameter and n is the system relative degree (here, $n = 2$). So, the specific surface becomes:

$$S_1(x_1) = \frac{de_1}{dt} + \delta_1 e_1 \tag{4}$$

To build the sliding surface, we establish this tracking error:

$$e_1 = C_{pv}(x_1 - x_1^*) \tag{5}$$

The time derivative of the error is obtained using (1. a):

$$\dot{e}_1 = \bar{i}_{pv} - x_2 - C_{pv}\dot{x}_1^* \tag{6}$$

By substituting the system dynamics (1. b), and incorporating (4) and (6), the time evolution S_1 can be expressed as follows:

$$\dot{S}_1(x_1) = \frac{di_{pv}}{dt} - \frac{1}{L}x_1 + \frac{1}{L}(1-u_1)\frac{x_3}{4} - C_{pv}\ddot{x}_1^* + \delta_1 i_{pv} - \delta_1 x_2 - \delta_1 C_{pv}\dot{x}_1^* \tag{7}$$

To compute the equivalent control law u_1^{eq}, we apply Utkin's technique, which involves setting $\dot{S}_1(x_1) = 0$. The equivalent control can be defined as

$$u_1^{Eq} = 1 + \frac{4}{x_3}\left[L\frac{di_{pv}}{dt} - x_1 - LC_{pv}\ddot{x}_1^* + \delta_1 L i_{pv} - \delta_1 L x_2 - \delta_1 L C_{pv}\dot{x}_1^*\right] \tag{8}$$

For designing the discontinuous part of the control, we take into consideration the following Lyapunov candidate function:

$$V_1 = \frac{1}{2}S_1(x_1)^2 \tag{9}$$

Its time derivative is given by

$$\dot{V}_1 = S_1\dot{S}_1 \tag{10}$$

The dynamic of Lyapunov is obtained by applying (2), (7), and (8) as follows:

$$\dot{V}_1 = -\frac{x_3}{4L}S_1(x_1)\, u_1^N \tag{11}$$

Convergence is guaranteed by imposing

$$\dot{V}_1 = -\eta_b\,|S_1(x_1)| \tag{12}$$

In (12), η_b is a positive gain, and since the sign function is defined as

$$sign(S_1) = \frac{|S_1(x_1)|}{S_1(x_1)} \tag{13}$$

where

$$sign(S) = \begin{cases} 1 & \text{if } S(x) > 0 \\ -1 & \text{if } S(x) < 0 \end{cases} \tag{14}$$

Eventually, the discontinuous control law u_b^N is expressed as:

$$u_1^N = \frac{4\eta_b L}{x_3} sign(S_1) \tag{15}$$

By bringing together the equivalent and discontinuous components (8),(15), the final sliding mode control law for MPPT is created in the following form:

$$u_1 = 1 + \frac{4}{x_3}\Big[L\frac{di_{pv}}{dt} - x_{_1} - LC_{pv}\ddot{x}_1^* + \delta_1 L i_{pv} - \delta_1 L x_2 - \delta_1 LC_{pv}\dot{x}_1^* + \eta_b L sign\left(S_1\right)\Big] \tag{16}$$

Remark. To reduce the chattering caused by the discontinuous nature of the sign function in the control law (16), it is replaced with a hyperbolic tangent function $\tanh(\cdot/\varepsilon)$, where ε is a small positive design parameter. This modification is suited for real-world implementation.

3.2 Design of Grid Current Regulator

To ensure seamless integration of the photovoltaic system into the grid, it is essential to accomplish effective PFC. This is achieved by precisely forcing the current to follow the grid voltage waveform. In this regard, the control goal is to regulate the grid-current x_5 to accurately follow its given intended signal $x_5^* = \beta v_{go}$, where β is a scaling signal that will be defined later in Sect. 3.3. This step uses u_g as the control input, applied at the inverter input. For this purpose, the sliding surface defined in (3) is now expressed considering that the relative degree of the system with respect to the grid current is $n = 1$. Therefore, the sliding surface is defined simply as

$$S_2\left(x_5\right) = e_2\left(x_5\right) \tag{17}$$

where $e_2\left(x_5\right) = L_g\left(x_5 - x_5^*\right)$ is the grid current tracking error between the actual one and its reference. Thus, its derivative leads to:

$$\dot{S}_2\left(x_5\right) = L_g\left(\dot{x}_5 - \dot{x}_5^*\right) \tag{18}$$

After substituting the system dynamics for the grid current (1. e) in (18), the sliding surface is written as:

$$\dot{S}_2\left(x_5\right) = -r_g x_5 - \bar{v}_{go} + \frac{x_4}{2} + \frac{x_3}{2}u_2 - L_g\dot{x}_5^* \tag{19}$$

To drive the equivalent control law u_2^{Eq}, we apply the Utkin method. Solving for u_2 results in the following formula:

$$u_2^{Eq} = \frac{2}{x_3}\left[r_g x_5 + \bar{v}_{go} - \frac{x_4}{2} + L_g\dot{x}_5^*\right] \tag{20}$$

This component keeps the system path on the mentioned surface.

To ensure convergence toward the surface, the Lyapunov function is designed as

$$V_2 = \frac{1}{2}S_2^2\left(x_5\right) \tag{21}$$

The derivative of this latter can be derived as

$$\dot{V}_2 = S_2\dot{S}_2 \tag{22}$$

Taking into consideration $\dot{S}_2$ and using the system dynamics and control decomposition, it concluded as:

$$\dot{S}_2\left(x_5\right) = \frac{x_3}{2}u_2^N \tag{23}$$

Thus, the Lyapunov derivative simplifies to

$$\dot{V}_2 = \frac{x_3}{2} S_2 u_2^N \tag{24}$$

To guarantee finite-time convergence, we impose:

$$\dot{V}_2 = \frac{x_3}{2} S_2 u_2^N = -\eta_g S_2 sign(S_2) \tag{25}$$

where η_g is a positive design parameter.

By following the same procedure detailed in Sect. 3.1, the resulting discontinuous term can be written as:

$$u_2^N = -\frac{2}{x_3} \eta_g sign(S_2) \tag{26}$$

Combining both the equivalent and discontinuous terms (20),(26), the proposed full sliding mode control law for the grid current is given by (27).

$$u_2 = \frac{2}{x_3} \left[r_g x_5 + \bar{v}_{go} - \frac{x_4}{2} + L_g \dot{x}_5^* - \eta_g sign(S_2) \right] \tag{27}$$

This control law ensures the grid current tracks its reference while maintaining robustness with a switching frequency equal to $50Khz$.

3.3 Design of DC-link Voltage Regulator

Since the DC-link voltage regulates the energy buffer between the PV source and the grid, its stability is essential for inverter operation and high-quality power injection. In this subsection, the objective is to uphold the DC-link voltage x_3 close to its reference x_3^*, even under varying environmental conditions. To this end, this loop controller generates the signal β, which scales the grid current reference $x_5^* = \beta v_g$ in such a way that it indirectly adjusts the grid-injected power to stabilize the DC-link voltage. To establish this relationship, it is assumed that the previous controlled loops are significantly quicker than the outer loop, and considering that the associated error dynamics (e_1, e_2) decay exponentially, the following simplified relation between β and the DC-link voltage is derived:

$$C \frac{dx_3^2}{dt} = 4 x_1 x_2 - 3\beta V_{go}^2 \tag{28}$$

To regulate the squared sum of the DC-link voltage, we define $y = \langle x_3^2 \rangle$ and its reference $y^* = (x_3^*)^2$. Accordingly, a filtered PI controller is employed to produce the control signal β, ensuring y tracks y^*. The resulting control law is expressed as

$$\beta(s) = \frac{a}{(a+s)\rho} \left[x_1 x_2 - \left(k_p + \frac{k_i}{s} \right) e_3 \right] \tag{29}$$

here, $e_3 = y^*(s) - y(s)$ represents the tracking error and $\rho = \frac{3}{4} V_{go}^2$ is a constant parameter, where s denotes the Laplace variable, and the PI regulator k_p, k_i are positive gains. This control structure ensures effective DC-link voltage regulation across the MLBC under dynamic operating conditions.

4 Simulation Results and Discussion

To implement the model of the proposed grid-connected PV system that has been designed in the above Sect. 3, it is now investigated using the SimPowerSystem toolbox in the MATLAB/Simulink environment to validate the performance of the controllers developed in this work.

For this simulation, the Solartech Power SPM210P (10 × 2) module is employed. The detailed parameters of the PV source are listed in Table 1. All parameter values used in the overall model are given in tables 2-3 to ensure full reproducibility. A comparative study involving a conventional PI controller has been performed to highlight the performance improvements achieved by the proposed approach. To evaluate the operation of the overall model and control scheme, two distinct scenarios are considered after $0.6s$, as described in the following subsections, where Sect 4.1 considers the performance with standard atmospheric conditions, and Sect 4.2 presents the performance with temperature variations; both of them take a constant DC-link voltage reference of 800 V.

Table 1. Electrical characteristics of the PV module.

Parameter	Symbol	Values
Maximum power voltage	V_m	30.1 V
Maximum power current	I_m	7.11 A
Maximum power	P_m	210 W
Short circuit current	I_{sc}	7.68 A
Open circuit voltage	V_{oc}	36.5 V

Table 2. The globally controlled system parameters.

Parameter	Symbol	Values
DC-DC converter	$C_{pv},\ L$	2 mF, 0.4 mH
DC-link converter	C	4 mF
Grid filter inductor	$L_g,\ r_g$	2 mH, 1 $\mu\Omega$
PWM Switching frequency	f_{sw}	10 kHz
AC Grid source frequency	$V_{go},\ f_g$	$220\sqrt{2}$ V, 50 Hz

Table 3. Key control design parameters.

Controller	Gains	Values
MPPT Regulator	$\delta_1,\ \eta_b,\ \varepsilon_b$	$3\times10^3,\ 1\times10^7,\ 0.005$
PFC Regulator	η_g	600
Filtered PI Regulator	$k_p,\ k_i,\ \alpha$	$10^{-2}\,\mathrm{V^{-2}\Omega^{-1}},\ 0.2\,\mathrm{V^{-2}\Omega^{-1}s^{-1}},\ 10^3\,\mathrm{s^{-1}}$

4.1 Scenario 1: Standard Condition

The cascaded nonlinear control strategy performance under standard weather conditions is illustrated in figure. 3. As shown in figure. 3(a), the PV voltage accurately tracks its reference, validating the efficiency of the MPPT regulator. The proposed controller shows better transient response and less overshoot when compared with the conventional PI controller, which shows sluggish settling, thereby validating the analytical results presented in the previous sections. Figure. 3(b) confirms that the DC-link voltage controlled by the outer-loop

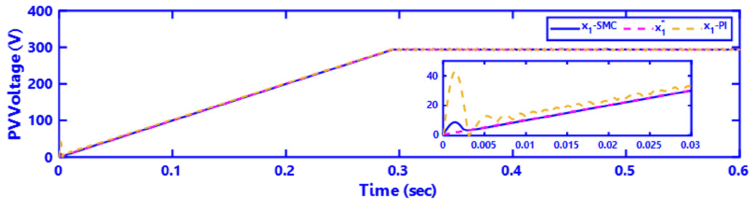

(a) Actual PV voltage and its reference

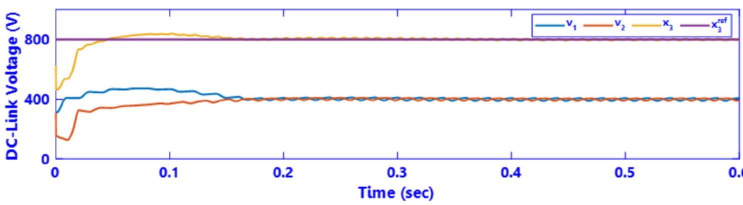

(b) DC-link voltage and its reference, with individual capacitor voltages

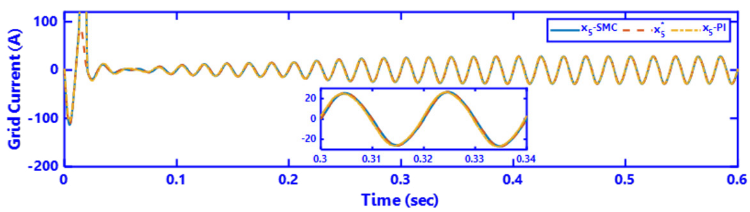

(c) Actual grid current and its reference

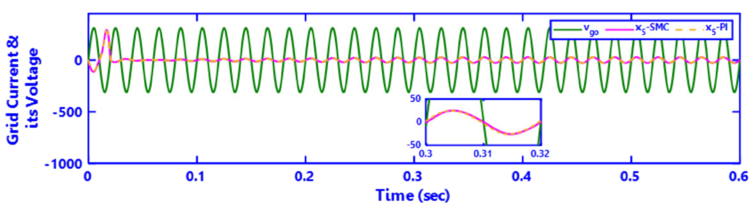

(d) Power factor correction (PFC) checking

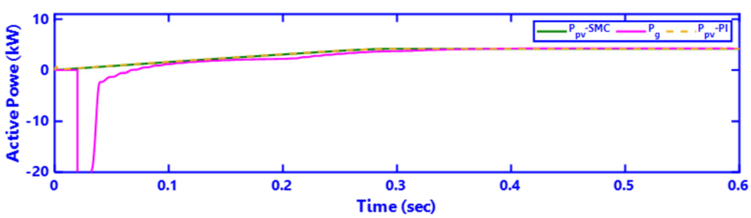

(e) Power injected into the grid from PV panels

Figure 3. System performance under standard conditions: (a) PV voltage, (b) DC-link voltage, (c) Grid current, (d) PFC, and (e) Grid-injected power.

filtered PI regulator remains stable and closely tracks its reference, with balanced voltage across both capacitors. In figure. 3(c), the grid current successfully tracks its sinusoidal reference, demonstrating the performance of the inner current control regulator, which remarks accuracy and consistency using SMC. In addition, figure. 3(d) demonstrates that unity power factor correction is achieved, as the voltage and current of the network remain in phase compared to the PI controller. Lastly, figure. 3(e) verifies that the power extracted from the PV panels is fully injected into the grid, confirming the overall effectiveness of the proposed control architecture.

4.2 Scenario 2: a Sudden Variation of Temperature

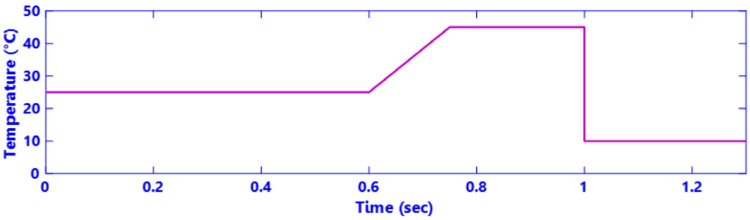

Figure 4. Temperature variation

Following the temperature variation ranging from T= 25°C to T= 45°C and then down to T= 10°C while maintaining the standard irradiation as illustrated in figure. 4, demonstrates the robustness of the proposed control strategy as depicted in figure. 5. Throughout these shifts, the PV voltage in the figure. 5(a) quickly reaches its updated MPPT reference, confirming the ability of the SMC-P&O-based regulator. The DC-link voltage profile in the figure. 5(b) remains stable and well-regulated, successfully tracking its reference, with balanced voltage across the two series capacitors. The grid current waveform in the figure. 5(c) follows its sinusoidal reference with precision. The power factor behavior in the figure. 5(d) indicates a unity PFC, as the current remains synchronized in phase with the voltage. Finally, the power transfer is shown in the figure. 5(e) verifies the full extracted power of PV power to the grid, proving the overall resilience of the cascaded control strategy under non-ideal conditions. In contrast, the PI-based controller exhibits a noticeably poorer transient response, characterized by slower settling and higher overshoot, which further confirms the effectiveness and robustness of the proposed control strategy.

5 Conclusion

In this letter, the SMC theory has been established for use on the power network connected to the PV system via electronic power MLBC-SIDO and an HBI with an RL filter. The multi-loop regulator is made to extract the maximum available power, inject a sinusoidal grid current with a unitary PFC, and use a filtered PI controller to regulate the DC link voltage to a fixed value. The excellent simulation results prove that the suggested control strategy meets the set objectives even under different weather conditions. The robustness of the proposed controller has been demonstrated through comparative analysis with a standard PI controller. Additionally, to validate the simulation results, future work will focus on the experimental implementation of the recently proposed circuit.

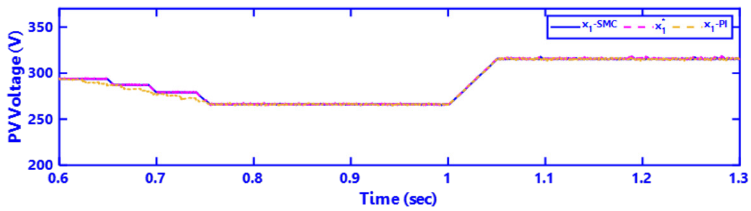

(a) Actual PV voltage and its reference

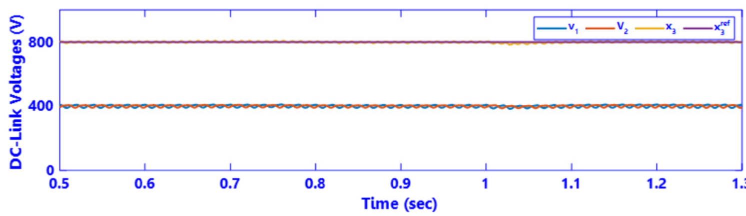

(b) DC-link voltage and its reference, with individual capacitor voltages

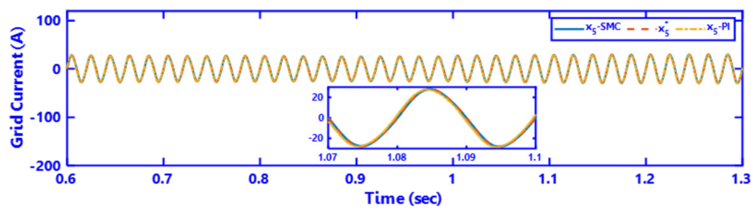

(c) Actual grid current and its reference

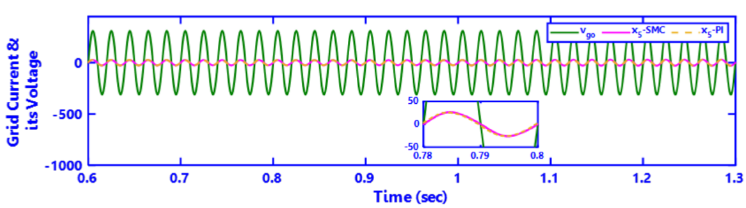

(d) Power factor correction (PFC) checking

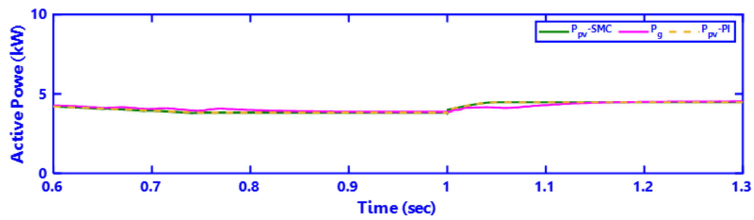

(e) Power injected into the grid from PV panels

Figure 5. System performance under temperature variation: (a) PV voltage, (b) DC-link voltage, (c) Grid current, (d) PFC, and (e) Grid-injected power.

References

1. S. Pawar, Harnessing the power of renewable energy: A study of sustainable sources and technologies, Journal for Research in Applied Sciences and Biotechnology **3**, 163 (2024). https://doi.org/10.55544/jrasb.3.4.19
2. N. Hourri, A. Abouloifa, Z. Hekss, I. Lachkar, O. Arich, A. El Boudali, Nonlinear Control of Three Phase Single Stage Grid Connected PV System Through Half Bridge Power Inverter, in *Automatic Control and Emerging Technologies* (Springer Nature Singapore, 2024), pp. 282–292
3. A. El Boudali, A. Abouloifa, I. Lachkar, M. Aourir, C. Aouadi, O. Arich, N. Hourri, Modeling and Control of Single-Phase Modular Multilevel Converter Using Backstepping Approach, in *Automatic Control and Emerging Technologies* (Springer Nature Singapore, 2024), pp. 808–816
4. J. Yang, R. Li, K. Ma, J. Xu, A distributed multimode control strategy for the cascaded dc–dc converter applied to mvac grid-tied pv system, IEEE Transactions on Industrial Electronics **70**, 2617 (2023). https://doi.org/10.1109/TIE.2022.3174300
5. H.C. Nannam, A. Banerjee, J.M. Guerrero, Analysis of an interleaved control scheme employed in split source inverter based grid-tied photovoltaic systems, IET Renewable Power Generation **15**, 1301 (2021). https://doi.org/10.1049/rpg2.12108
6. Z. Yao, M. Liu, Y. Li, Z. Xiao, Y. Jiang, L. Zhang, Y. Tang, Generalized trapezoidal current mode-based zero-voltage switching for multilevel dc–dc converters, IEEE Transactions on Power Electronics **40**, 8956 (2025). https://doi.org/10.1109/TPEL.2025.3551341
7. O. Hamada, M.A.Y. Abdalla, S.A. Ibrahim, Hybrid Single Inductor Multiple-Output Boost DCDC Converter with Digital Adaptive Inductor Peak Current Control, in *2024 6th Novel Intelligent and Leading Emerging Sciences Conference (NILES)* (IEEE, 2024), pp. 377–380
8. O. Arich, A. Abouloifa, I. Lachkar, S. Echalih, M. Aourir, A. El Boudali, N. Hourri, Nonlinear Controller Design for Photovoltaic Powered Single-Inductor Dual-Output Boost DC–DC Converter, in *Automatic Control and Emerging Technologies* (Springer Nature Singapore, 2024), pp. 475–484
9. O. Arich, A. Abouloifa, A. El Boudali, M.S. Al Numay, A. El Aroudi, A multi-loop nonlinear control approach for a reduced-switch-count grid-tied pv system, Electric Power Systems Research **260**, 113352 (2026). https://doi.org/10.1016/j.epsr.2026.113352
10. M. Mousa, M.E. Ahmed, M. Orabi, New Converter Circuitry for PV Applications Using Multilevel Converters, in *INTELEC 2009 - 31st International Telecommunications Energy Conference* (IEEE, 2009), pp. 1–6
11. N.R. Sulake, A.K. Devarasetty Venkata, S.B. Choppavarapu, Fpga implementation of a three-level boost converter-fed seven-level dc-link cascade h-bridge inverter for photovoltaic applications, Electronics **7**, 282 (2018). https://doi.org/10.3390/electronics7110282
12. G. Tahri, F. Tahri, A. Tahri, Fractional order pid controller design of a dc–dc multilevel boost converter using the nelder-mead optimization, International Journal of Power Electronics and Drive Systems **15**, 2409 (2024). https://doi.org/10.11591/ijpeds.v15.i4.pp2409-2421
13. S. El Islam Remache, K. Barra, Performance Comparison Among Boost and Multilevel Boost Converters for Photovoltaic Grid Connected System Using Finite Set Model Predictive Control, in *2018 9th International Renewable Energy Congress (IREC)* (IEEE, 2018), pp. 1–6

14. M. Maalandish, S. Pourjafar, S.H. Hosseini, N. Taghizadegan Kalantari, Leakage current elimination with improved non-isolated nine-level inverter for grid-connected pv panels, Journal of Energy Management and Technology **1**, 46 (2017). https://doi.org/10.22109/jemt.2017.83238.1008
15. R. Malathi, S. Lavanya, K. Umapathy, M.A. Archana, T.D. Kumar, S. Omkumar, Closed Loop Sliding System with Grid Connectivity for PV Inverter Using Controlled Quadratic Boost Converter, in *2025 International Conference on Electronics and Renewable Systems (ICEARS)* (IEEE, 2025), pp. 215–220